The structure of oceanic core complexes controlled by the depth distribution of magma emplacement

Jean-Arthur Olive[1]*[†], Mark D. Behn[2] and Brian E. Tucholke[2]

At mid-ocean spreading centres, extension can be accommodated by slip on large, long-lived (1–2 Myr) detachment faults that expose large tracts of lower crustal gabbroic rocks and mantle peridotite. These structures are known as oceanic core complexes. The development of detachment faults is controlled by the rate at which magma is injected into the brittle lithosphere as intrusive dykes. Recent modelling studies suggested that oceanic core complexes form under low magma injection rates, when only 30–50% of total plate separation is accommodated by the injection of magma into the lithosphere[1–3]. Yet, paradoxically, field observations[4–11] document oceanic core complexes that have formed under a spectrum of magma injection rates, from amagmatic to fully magmatic conditions. Here we present a numerical model of oceanic core complex formation that explicitly considers magma intrusion not only in the brittle lithospheric layer, as in earlier simulations[1–3], but also in the underlying ductile asthenosphere. We find that the rate of magma intrusion into the brittle layer controls fault evolution, whereas the rate of intrusion below the brittle–ductile transition has no influence on fault development, but controls the volume of gabbro exhumed. Our findings suggest that oceanic core complexes can form under high magma intrusion rates if intrusion is accommodated mainly by the ductile asthenosphere, thus reconciling the disparity between prevailing models and field observations.

The amount of melt supplied to a mid-ocean ridge (MOR) spreading segment is a key control on the development of normal faults[1–3,12,13]. Faults in turn control the redistribution of crustal lithologies and specifically, at slower-spreading MORs, the locations where mafic plutons and ultramafic mantle rocks are exhumed. Of particular interest are long-lived detachment faults with footwalls that form domed, corrugated megamullions that represent fully developed oceanic core complexes (OCCs) and expose a variety of rock types. At the apparently magmatic end of the spectrum, Atlantis Bank on the southwest Indian ridge exposes a continuous gabbro section that extends >10 km along plate flow lines and is >1.5 km thick[6]. In contrast, extensive exposures of mantle peridotite with more restricted, embedded gabbro plutons occur in OCCs on the Mid-Atlantic Ridge[7–11,14], suggesting reduced and/or more intermittent magma supply. Furthermore, although hanging walls of OCCs have been poorly studied, they seem to show little structural/morphologic variation, which suggests that they may have relatively uniform composition compared with variations in the OCC footwalls. These features suggest not only that melt supply to detachment footwalls is strongly four-dimensional, but also that melt may be partitioned differently above and below the brittle–ductile transition (BDT).

In this study, we use geodynamic models to quantitatively investigate the interplay between faulting and patterns of melt emplacement at MORs by varying both the rate and location of melt injection. Seafloor spreading is simulated by symmetrically extending a two-dimensional model domain while widening a central 'magma injection zone' of height H_B and H_D above and below the BDT, respectively (Fig. 1; see the Methods section). Crust and mantle lithologies are tracked throughout each model run, and we distinguish between materials injected above and below the BDT as brittle- and ductile-injected crust (BIC and DIC), respectively. We focus on the effects of (1) decoupling the magma supply within the brittle lithosphere (expressed as the ratio of magmatic to total extension, M_B) from that in the underlying ductile asthenosphere (M_D), and (2) temporal variability in magma supply on fault development and on the spatial distribution of crustal and mantle lithologies.

A series of simulations was carried out with different combinations of injection parameters (H_B, M_B, H_D and M_D). Consistent with previous studies[1–3], we find that OCCs develop by detachment faulting in simulations where $M_B \approx 0.3$–0.5. At $M_B = 0.5$, OCC formation results in a systematic pattern of crustal emplacement in which BIC is accreted solely on the conjugate side, leaving a remnant BIC hanging wall block adjacent to the seafloor trace of the detachment fault that forms the OCC (Fig. 1). DIC, however, is distributed equally between the OCC side, where it is exhumed in the footwall of the detachment, and the conjugate side, where it is emplaced below the BIC.

Growth of a detachment fault is not affected by the imposed value of M_D (Fig. 1a,b) or by changes in M_D through time (Fig. 1c). However, changes in M_D directly control the amount of DIC that is exhumed in the OCC and emplaced in the ductile layer on the conjugate side. Similarly, changing only H_D (not shown) affects the thickness of the DIC layer in the OCC as well as the ratio of BIC versus DIC emplaced on the conjugate side, but it does not change the overall pattern of faulting.

We quantified our results over a range of injection parameters (H_B, M_D and H_D) by comparing the total crustal thickness (BIC + DIC) 10 km off-axis on the detachment (t_d) and conjugate (t_c) sides of the ridge axis for a series of model runs with M_B held fixed at 0.5 (Fig. 1a). A simple mass balance calculation is used to predict crustal thickness variations across an OCC as a function of H_B, M_D and H_D. Assuming symmetric spreading about the ridge axis, the total thickness of BIC and DIC emplaced within the injection zone will be $2M_B H_B$ and $2M_D H_D$, respectively. However,

[1]Département Terre-Atmosphère-Océan, Ecole Normale Supérieure, Paris 75005, France, [2]Department of Geology and Geophysics, Woods Hole Oceanographic Institution, Woods Hole, Massachusetts 02543, USA. [†]Present address: Massachusetts Institute of Technology/Woods Hole Oceanographic Institution Joint Program in Oceanography, Cambridge, Massachusetts 02139 USA. *e-mail: jaolive@mit.edu.
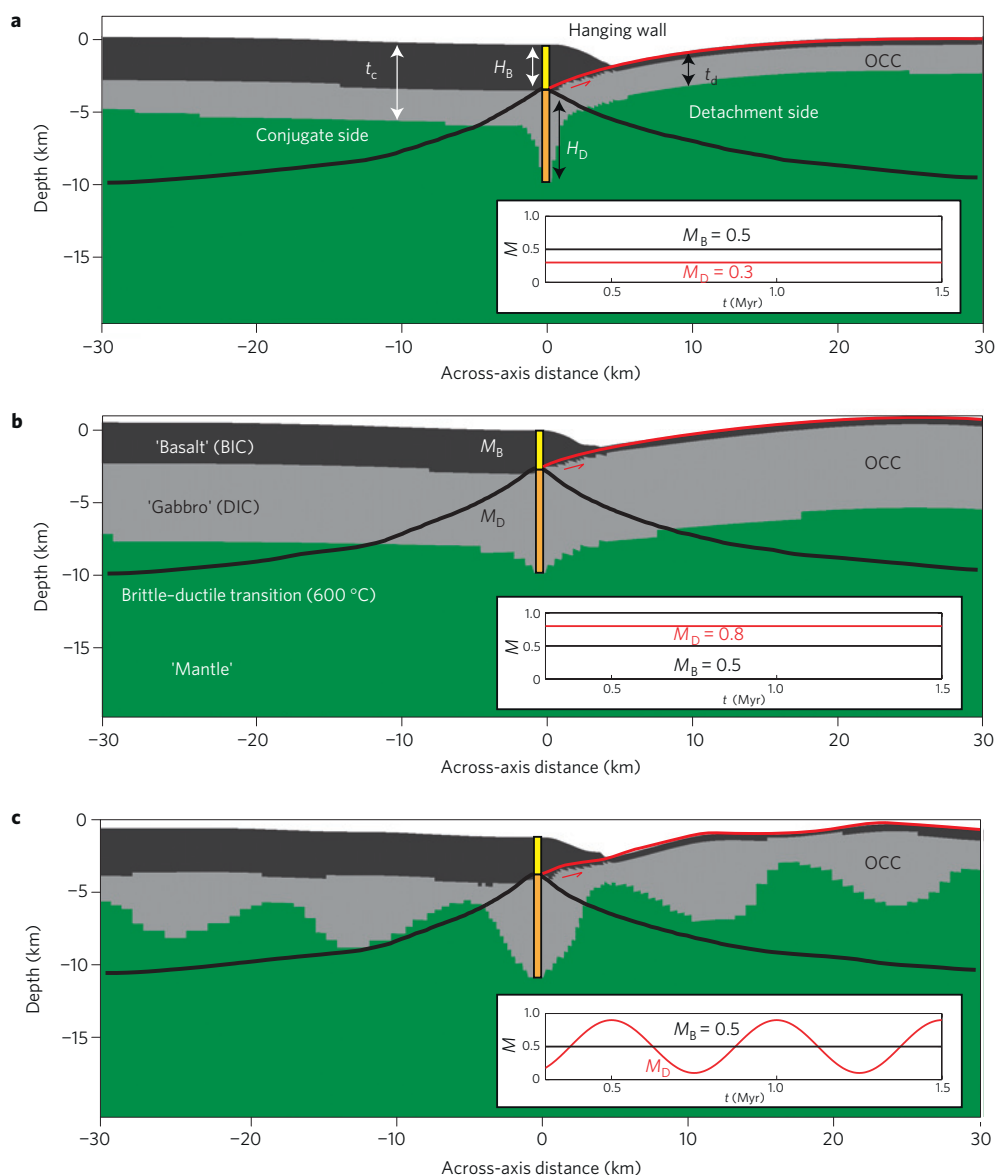
Figure 1 | Modelled faulting and partitioning of volcanic, plutonic and mantle materials during OCC growth. a–c, Distribution of BIC (black), DIC (grey) and mantle (green) lithologies after 1.5 Myr of spreading in cases where $M_B = 0.5$ and a detachment fault develops continuously. M_D varies from 0.3 (**a**) to 0.8 (**b**) and in **c** it oscillates between 0.1 and 0.9 with a period of 0.5 Myr. In these runs, $H_B + H_D = 10$ km, with $H_B \sim 3$ km. The BDT separating BIC and DIC (yellow and orange parts of the central dyke, respectively) corresponds to the 600 °C isotherm (thick black line).

because the hanging wall of the detachment does not grow, the BIC must accrete solely on the conjugate side, whereas the DIC is equally partitioned across the ridge axis. Thus, for $M_B = 0.5$ the crustal thickness expected on the detachment and conjugate sides is $t_d = M_D H_D$ and $t_c = H_B + M_D H_D$, respectively. These simple mass balance relations do an excellent job of predicting the numerical results over a wide range of H_B, M_D and H_D (Fig. 2).

We also investigated several cases where $M_B \neq 0.5$ (Fig. 3). For simplicity, we fixed $M_B = M_D = M$ in these simulations, but we note that emplacement may be more complex when $M_B \neq M_D$. For $M_B = 0.4$, a long-lived detachment forms, but the detachment surface is dissected by steep, mostly outward-dipping normal faults that offset both the BIC and DIC layers (Fig. 3b). Total crustal thickness on each plate remains fairly constant through time, but a portion of BIC that normally would accrete on the conjugate is transferred to the OCC. This is apparently caused by the detachment migrating towards the axis and crossing the injection zone where it takes up, by tectonic extension, the accretion deficit on the

conjugate. As M_B decreases further to 0.2 (Fig. 3a), random on-, off- and cross-axis faulting becomes the normal style of extension, both DIC and BIC are transferred irregularly between plates and mantle can be exhumed; this results in a very complex structure and distribution of lithologies. In contrast, when M_B is >0.5, a continuous crustal layer is produced on both plates. In this case, the thickness of the DIC layer is essentially constant but the BIC is thinned by faults that alternate back and forth across the ridge axis (Fig. 3c).

The key finding in this study is that differing rates of magma intrusion in the brittle and ductile regimes control both the patterns of faulting and the distribution of igneous lithologies at MORs in a systematic manner. Specifically, we show that the entire range of synkinematic DIC intrusion rates ($M_D = 0$–1) is compatible with detachment fault growth, provided that BIC intrusion rates are in the critical range (M_{Bcrit}) of 0.5 to ~0.3. Introducing a depth-variable rate of magma intrusion reconciles the intermediate rate of dyking needed to allow detachment faulting in the lithosphere with
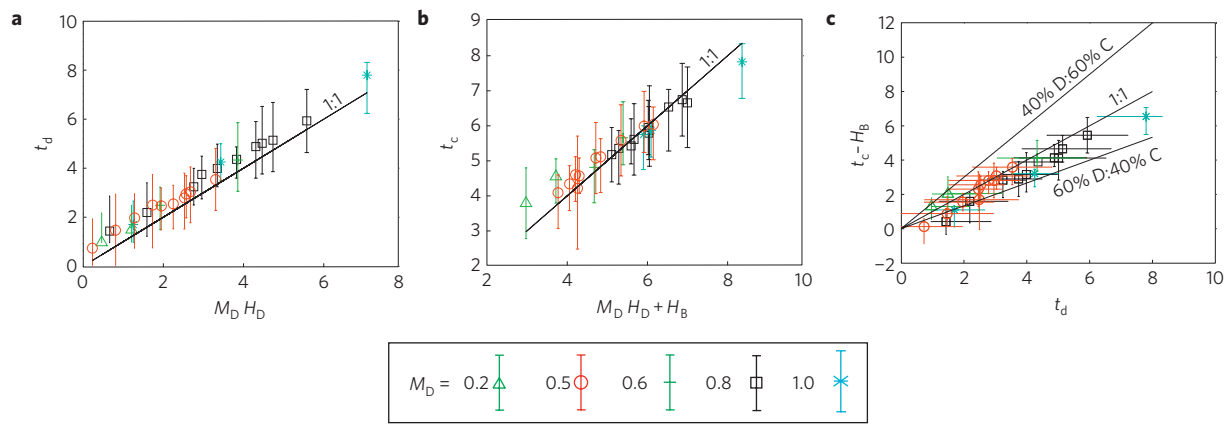
Figure 2 | Predicted crustal thicknesses as a function of the injection parameters. Total crustal thickness (BIC + DIC) on the detachment (t_d) and conjugate (t_c) sides of the ridge axis from a suite of model runs with fixed $M_B = 0.5$ and various M_D (0.2–1.0), H_B (1–3 km) and H_D (1–7 km). **a,b**, The scaling laws (1:1 line) predicting t_d and t_c. **c**, Comparison of DIC thickness in the footwall of the detachment (D) versus the conjugate side (C). The 1:1 line corresponds to symmetric DIC emplacement and the other two lines show 40% and 60% asymmetry on either side, respectively. The error bars measure uncertainties associated with numerical smoothing when assigning material identities to the elements, and are typically 1 or 2 element-size.
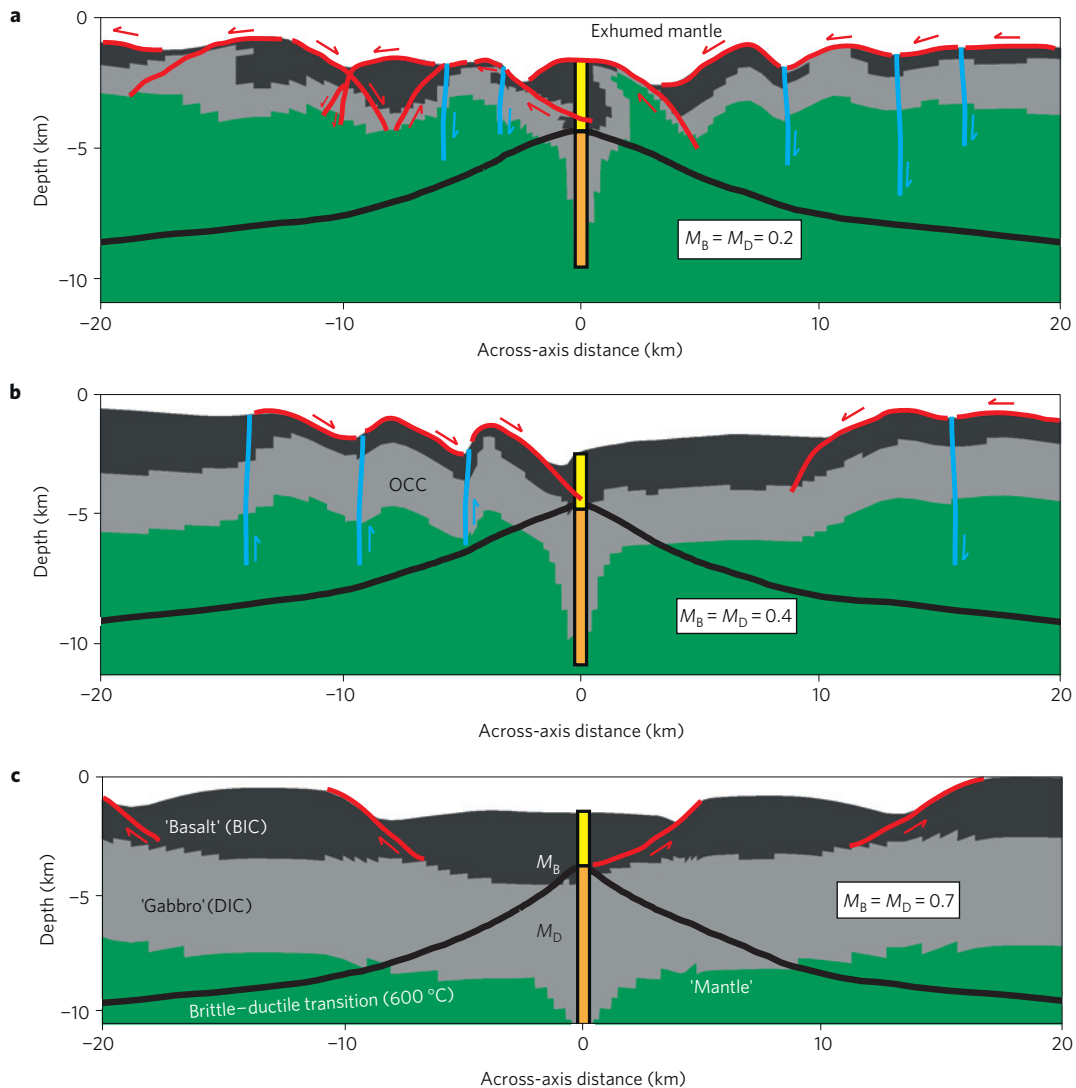

Figure 3 | Modelled faulting and partitioning of volcanic, plutonic and mantle materials as a function of melt supply. a–c, Model snapshots at 1.5 Myr for cases where $M_B = M_D = 0.2$ (**a**), 0.4 (**b**) and 0.7 (**c**). In these runs, $H_B + H_D = 9$ km, with $H_B \sim 2$–3 km. First- and second-generation fault surfaces are shown in red and blue, respectively. Other conventions are as in Fig. 1.
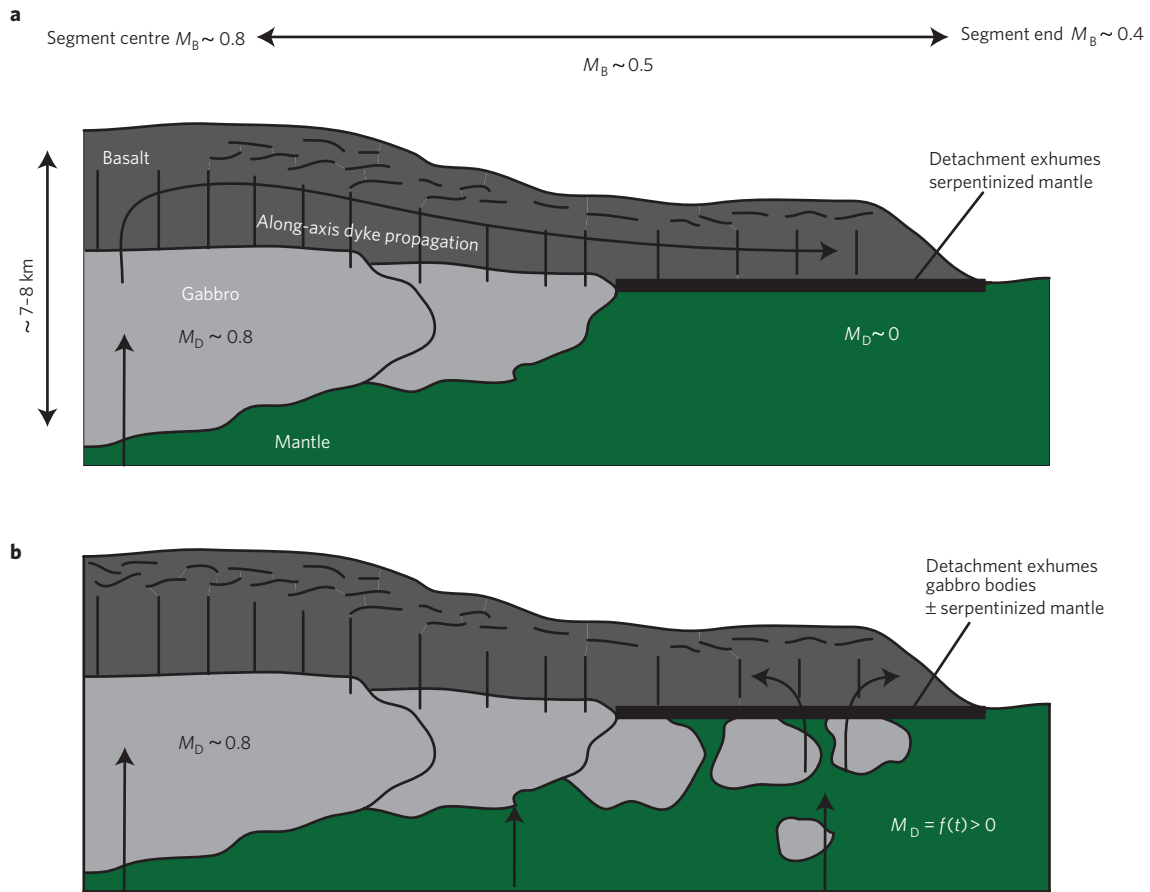
Figure 4 | Endmember models for detachment faulting and melt distribution at the segment scale. In these along-axis scenarios, a long-lived detachment fault (bold line) forms at the along-axis position where melt supply to the brittle layer is in the critical range ($M_{Bcrit} = 0.5$ to $\sim$0.3) needed for detachment faulting. **a**, Scenario in which melt is supplied entirely by along-axis dyke propagation from the segment centre, little or no melt is derived from below the detachment and mantle is exhumed along a dyke–mantle contact. **b**, Scenario in which M_{Bcrit} is satisfied by melt derived from intrusions below the detachment and gabbro plutons are exhumed in the OCC along a dyke–gabbro contact.

either amagmatic exhumation of large tracts of mantle ($M_D \sim 0$) or synkinematic emplacement of gabbroic bodies at virtually any scale ($M_D = f(t) > 0$) in the footwalls of OCCs. A corollary to this result is that emplacement of a large gabbro body will trigger OCC termination only if it results in increased rates of dyking ($M_B > 0.5$) in the brittle lithosphere.

We propose two endmember scenarios for depth-variable magma injection rates (Fig. 4). In the first, dyke intrusion in the brittle lithosphere occurs by along-axis propagation from a magma-rich segment centre towards the segment end[15] (Fig. 4a). In this scenario, M_B declines into the detachment-forming range, M_{Bcrit}, towards segment ends, where most OCCs are found[5]. Dykes above the detachment are not fed from below because the colder thermal regime inferred in these areas favours melt crystallization at depth rather than eruption[16]. As a consequence, primarily mantle is exhumed by a detachment fault that is located at the dyke–mantle transition. This kind of structural/lithological relationship has been interpreted at the Kane megamullion[9].

In the second scenario, dykes are fed from underlying gabbro intrusions (Fig. 4b). M_{Bcrit} could be satisfied anywhere within the segment, but it might be more likely to be found away from the more magmatically robust segment centre, and thus towards the segment end. Of course M_{Bcrit} could also be achieved by some combination of lateral and vertical dyking represented by these two endmembers. It is noteworthy that this spectrum of scenarios accommodates a wide variety of temperature and intrusion conditions in the detachment footwall, which may explain why very different kinds

of temperature/deformation history have been documented in different OCCs (for example, refs 9,17).

Although our simulations involve continuous crustal layers, OCCs tend to exhume discrete gabbro bodies surrounded by serpentinized peridotite[7,9]. This probably reflects both spatial (along-axis) and temporal (across-axis) variations in gabbro intrusion rates. Along-axis variations in gabbro layer thickness can be accounted for in our simulations by variations in either M_D (reflecting differences in melt supply) or H_D (reflecting variations in axial thermal structure, which will in turn be influenced by magma supply and/or the efficiency of hydrothermal cooling). Our model also predicts that gabbro exhumed in an OCC should be matched by an equal volume of gabbro in the conjugate plate, below volcanics and sheeted dykes of the upper crust, provided that far-field extension is symmetric about the ridge axis, which may not be the case for all OCCs. This prediction can be tested by detailed seismic and gravity studies across both an OCC and its conjugate hanging wall.

Temporal variability in melt supply in slow-spreading crust is well established. Cycling between relatively magmatic and amagmatic conditions often seems to occur on the Mid-Atlantic Ridge at periods of $\sim$2–4 Myr (refs 18,19) possibly reflecting heterogeneities in mantle fertility. Interestingly, most OCCs in the form of megamullions develop over about 1–2 Myr (ref. 5), which may suggest that M_{Bcrit} is achieved over about half the period of the large-scale magmatic cycles. Shorter-period magmatic cyclicity also occurs on timescales down to 80–160 kyr (ref. 20) and may be associated with the dynamics of magma ascent, storage and eruption. These

fluctuations are probably responsible for the development of discrete gabbro bodies within OCCs, as illustrated by the model in Fig. 1c. Our model predicts that a detachment formed under these fluctuating conditions will exhibit small oscillations in OCC footwall topography (of the order of 150 m for 4 km variations in gabbro layer thickness, as shown Fig. 1c) because of the isostatic and flexural effects of intruding gabbro plutons that are less dense than the surrounding mantle. Such flexural effects may contribute to high-angle off-axis faulting of the footwall, which is often observed[5].

Our modelling results provide a new conceptual framework to interpret relations between magmatism and faulting at slow- to intermediate-spreading MORs. Specifically, we argue that fault style is primarily controlled by the rate of dyking in the brittle lithosphere, whereas lithologic variations in both the brittle lithosphere and in the underlying ductile asthenosphere are controlled separately by intrusion rates that are unique to each layer. Our results allow us to interpret OCC formation in the context of both rate and location of melt supply at the segment scale and in a four-dimensional framework. Future modelling studies should focus on the tectonic effects of along-axis variability in melt supply to gain improved insight into segment-scale interrelations between tectonism, lithology and hydrothermal circulation.

Methods

We use the Fast Lagrangian Analysis of Continua technique to solve for conservation of mass, momentum and heat[3,12,21–23], (see ref. 2 for an extensive description) in a 60-km-wide by 20-km-deep domain representing a vertical cross-section of a MOR that is spreading symmetrically at a half-rate $U_s = 2.5\,\mathrm{cm\,yr}^{-1}$.

Material deforms following a dry-diabase rheology[24], which is effectively elastic-plastic above the 600 °C isotherm (equivalent to the BDT) and visco-elastic below. Plastic yielding occurs in the brittle layer when a Mohr–Coulomb criterion is met, and cohesion is lost as plastic strain accumulates, which allows the development of localized deformation (faults).

The Fast Lagrangian Analysis of Continua method employs a Lagrangian description of the deformation field. This results in the distortion of model elements as they accumulate strain resulting from faulting or magma injection, causing a loss of numerical accuracy. To circumvent this problem, we regrid the model domain whenever the distortion of an element reaches a critical threshold. All variables of interest are then linearly interpolated from the old (deformed) grid to the new (undeformed) grid[23].

Magma injection is modelled by applying a stress perturbation on a fixed central column of elements over one numerical time step[1–3]. Heat is simultaneously added to the ridge axis, accounting for both the injection temperature of the magma (1,200 °C) and the latent heat of crystallization[2]. The effective 'magmatic spreading' can be regarded as the relaxation of the quantum elastic perturbation, which results in net horizontal widening of the column, pushing on the surrounding material at a rate proportional to the spreading half-rate: above the BDT, BIC was added at a rate $U_B = 2\,M_B U_s$, whereas DIC was added below at a rate $U_D = 2\,M_D U_s$. The total height of the injection zone ($H = H_B + H_D$) was defined for each model run, but the relative heights of brittle (H_B) and ductile (H_D) injection evolve with the thermal structure. Magma injection is therefore fully described by a set of four independent parameters, namely the vertical height and rate of brittle (H_B and M_B) and ductile (H_D and M_D) injection (see Fig. 1a,b). We consider that the BIC is representative of upper-crustal volcanics and sheeted dykes, whereas the DIC represents gabbroic plutons intruded beneath the BDT. This simplified method for gabbro emplacement results in a constant accretion rate with depth and is independent of the specific lower-crust emplacement model (for example, gabbro glacier versus multiple sills).

To effectively track lithologies throughout a model run and investigate the crustal emplacement patterns, we assigned an identity number to new materials at each location where they entered the model space: (1) BIC, (2) DIC and (3) new mantle, which upwells through the base of the domain. Numerical smearing associated with regridding may produce the artefact of a thin (~2 element size) carapace of BIC on the footwall of long-lived faults (see Fig. 1).

References

1. Buck, W. R., Lavier, L. L. & Poliakov, A. N. B. Modes of faulting at mid-ocean ridges. *Nature* **434,** 719–723 (2005).
2. Behn, M. D. & Ito, G. Magmatic and tectonic extension at mid-ocean ridges: 1. Controls on fault characteristics. *Geochem. Geophys. Geosyst.* **9,** Q08010 (2008).
3. Tucholke, B. E., Behn, M. D., Buck, W. R. & Lin, J. Role of melt supply in oceanic detachment faulting and formation of megamullions. *Geology* **36,** 455–458 (2008).
4. Tucholke, B. E. & Lin, J. A geological model for the structure of ridge segments in slow spreading ocean crust. *J. Geophys. Res.* **99,** 11937–11958 (1994).
5. Tucholke, B. E., Lin, J. & Kleinrock, M. C. Megamullions and mullion structure defining oceanic metamorphic core complexes on the Mid-Atlantic Ridge. *J. Geophys. Res.* **103,** 9857–9866 (1998).
6. Dick, H. J. B. *et al.* A long *in situ* section of the lower ocean crust: Results of ODP Leg 176 drilling at the Southwest Indian Ridge. *Earth Planet. Sci. Lett.* **179,** 31–51 (2000).
7. Blackman, D. K. *et al.* Geology of the Atlantis Massif (Mid-Atlantic Ridge, 30° N): Implications for the evolution of an ultramafic oceanic core complex. *Mar. Geophys. Res.* **23,** 443–469 (2002).
8. MacLeod, C. J. *et al.* Direct geological evidence for oceanic detachment faulting: The Mid-Atlantic Ridge, 15°45′ N. *Geology* **30,** 879–882 (2002).
9. Dick, H. J. B., Tivey, M. A. & Tucholke, B. E. Plutonic foundation of a slow-spreading ridge segment: Oceanic core complex at Kane Megamullion, 23°30′ N, 45°20′ W. *Geochem. Geophys. Geosyst.* **9,** Q05014 (2008).
10. MacLeod, C. J. *et al.* Life cycle of oceanic core complexes. *Earth Planet. Sci. Lett.* **287,** 333–344 (2009).
11. Xu, M., Canales, J. P., Tucholke, B. E. & DuBois, D. L. Heterogeneous seismic velocity structure of the upper lithosphere at Kane oceanic core complex, Mid-Atlantic Ridge. *Geochem. Geophys. Geosyst.* **10,** Q10001 (2009).
12. Behn, M. D., Buck, W. R. & Sacks, I. S. Topographic controls on dike injection in volcanic rift zones. *Earth Planet. Sci. Lett.* **246,** 188–196 (2006).
13. Ito, G. & Behn, M. D. Magmatic and tectonic extension at mid-ocean ridges: 2. Origin of axial morphology. *Geochem. Geophys. Geosyst.* **9,** Q09012 (2008).
14. Canales, J. P., Tucholke, B. E., Xu, M., Collins, J. A. & DuBois, D. L. Seismic evidence for large-scale compositional heterogeneity of oceanic core complexes. *Geochem. Geophys. Geosyst.* **9,** Q08002 (2008).
15. Fialko, Y. A. & Rubin, A. M. Thermodynamics of lateral dike propagation: Implications for crustal accretion at slow-spreading ridges. *J. Geophys. Res.* **103,** 2501–2514 (1998).
16. Cannat, M. How thick is the magmatic crust at slow spreading oceanic ridges? *J. Geophys. Res.* **101,** 2847–2857 (1996).
17. Escartin, J., Mevel, C., MacLeod, C. J. & McCaig, A. M. Constraints on deformation conditions and the origin of oceanic detachments: The Mid-Atlantic Ridge core complex at 15°45′ N. *Geochem. Geophys. Geosyst.* **4,** 1067 (2003).
18. Bonatti, E. *et al.* Mantle thermal pulses below the Mid-Atlantic Ridge and temporal variations in the formation of oceanic lithosphere. *Nature* **423,** 499–505 (2003).
19. Tucholke, B. E. *et al.* Segmentation and crustal structure of the western Mid-Atlantic Ridge flank, 25° 25′–27° 10′ N and 0–29 m.y. *J. Geophys. Res.* **102,** 10203–10223 (1997).
20. Canales, J. P., Collins, J. A., Escartin, J. & Detrick, R. S. Seismic structure across the rift valley of the Mid-Atlantic Ridge at 23° 20′ (MARK area): Implications for crustal accretion processes at slow-spreading ridge. *J. Geophys. Res.* **105,** 28411–28425 (2000).
21. Cundall, P. A. Numerical experiments on localization in frictional materials. *Ingenieur-Archiv.* **59,** 148–159 (1989).
22. Poliakov, A. N. B. & Buck, W. R. in *In Faulting and Magmatism at Mid-Ocean Ridges* (eds Buck, W. R., Karson, J. A. & Lagabrielle, Y.) 305–323 (American Geophysical Union, 1998).
23. Lavier, L. L. & Buck, W. R. Half-graben versus large-offset low-angle normal fault: Importance of keeping cool during normal faulting. *J. Geophys. Res.* **107,** 2122 (2002).
24. Mackwell, S. J., Zimmerman, M. E. & Kohlstedt, D. L. High-temperature deformation of dry diabase with application to tectonics on Venus. *J. Geophys. Res.* **103,** 975–984 (1998).

Author contributions

J-A.O. and M.D.B. carried out the modelling and B.E.T. advised on geological interpretations. J-A.O. took the lead in writing the manuscript; M.D.B. and B.E.T. provided comments and revisions.